Article

Cell

# The Fuzzy Logic of Network Connectivity in Mouse Visual Thalamus

## Graphical Abstract

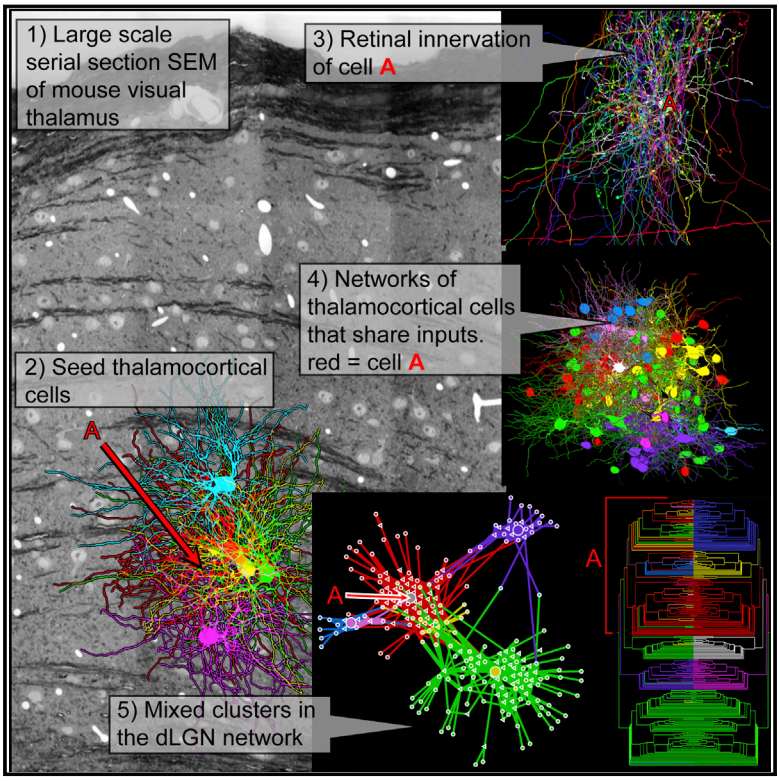


## Authors

Josh Lyskowski Morgan, Daniel Raimund Berger, Arthur Willis Wetzel, Jeff William Lichtman

## Correspondence

joshmorgan@fas.harvard.edu (J.L.M.), jeff@mcb.harvard.edu (J.W.L.)

## In Brief

A connectomic study in mouse thalamus revealed an unexpectedly complex network. Different kinds of retinal cells innervated individual target cells, individual retinal cells innervated different kinds of target cells, and connectivity varied between dendrites belonging to one cell.

## Highlights

- Connectomic analysis in the LGN revealed an unexpectedly complex network
- Structurally distinct RGCs and TCs could not be divided into distinct pathways
- Connectivity varied between the dendrites belonging to one thalamocortical cell
- The structure and connectivity of TCs defied strict typological categorization

Morgan et al., 2016, Cell *165*, 192–206
March 24, 2016 ©2016 Elsevier Inc.
http://dx.doi.org/10.1016/j.cell.2016.02.033

CellPress

Cell

Article

# The Fuzzy Logic of Network Connectivity in Mouse Visual Thalamus

Josh Lyskowski Morgan,[1,*] Daniel Raimund Berger,[1] Arthur Willis Wetzel,[2] and Jeff William Lichtman[1,*]
[1]Department of Molecular and Cellular Biology and Center for Brain Science, Harvard University, Cambridge, MA 02138, USA
[2]Pittsburgh Supercomputing Center, Pittsburgh, PA 15213, USA
*Correspondence: joshmorgan@fas.harvard.edu (J.L.M.), jeff@mcb.harvard.edu (J.W.L.)
http://dx.doi.org/10.1016/j.cell.2016.02.033

## SUMMARY

**In an attempt to chart parallel sensory streams passing through the visual thalamus, we acquired a 100-trillion-voxel electron microscopy (EM) dataset and identified cohorts of retinal ganglion cell axons (RGCs) that innervated each of a diverse group of postsynaptic thalamocortical neurons (TCs). Tracing branches of these axons revealed the set of TCs innervated by each RGC cohort. Instead of finding separate sensory pathways, we found a single large network that could not be easily subdivided because individual RGCs innervated different kinds of TCs and different kinds of RGCs co-innervated individual TCs. We did find conspicuous network subdivisions organized on the basis of dendritic rather than neuronal properties. This work argues that, in the thalamus, neural circuits are not based on a canonical set of connections between intrinsically different neuronal types but, rather, may arise by experience-based mixing of different kinds of inputs onto individual postsynaptic cells.**

## INTRODUCTION

Serial section electron microscopy (EM) provides access to the full patterns of synaptic connections linking nerve cells together. Because the heavy metal stains used for electron contrast label all cell membranes, circuit tracing in serial EM reveals the actual cohorts of presynaptic axons that connect to a postsynaptic cell. By exploring collateral branches of these same axons, one can also learn how axons distribute their innervation among all the postsynaptic cells in a region of the brain. We used this approach to describe what we expected to be one of the most straightforward CNS pathways: the connections between retinal ganglion cells (RGCs) and thalamic neurons projecting to cerebral cortex. Previous evidence suggested that the lateral geniculate nucleus (LGN) network might be relatively easy to understand. First, several studies argue that only a few RGC axons innervate each thalamocortical neuron (TC) (Cleland et al., 1971; Hamos et al., 1987; Mastronarde, 1992; Usrey et al., 1999; Chen and Regehr, 2000; Hong et al., 2014). Consistent with low convergence, receptive field properties of TCs and RGCs are similar (Grubb and Thompson, 2003). Moreover, each functional class of TC seems to be driven by a corresponding functional class of RGC. For example, in the cat, the three main physiological classes of thalamic neurons (X, Y, and W) reflect responses that correspond to X, Y, and W cells in the retina (Sherman and Spear, 1982). In cats and macaque, the response properties of TCs precisely match the receptive field properties of the RGCs that innervate them (Lee et al., 1983). These results imply that different classes of RGCs selectively innervate different classes of TCs. This idea is strengthened by evidence that TCs have distinct dendritic geometries, which correspond to X-like, Y-like, and W-like response properties (Friedlander et al., 1981). Moreover, different classes of RGCs have distinct synaptic properties, geometries, and stratification depths in the LGN (Dhande and Huberman, 2014 for review) and functionally distinct regions of the mouse LGN project to different layers of the cortex (Cruz-Martín et al., 2014). The overwhelming impression from this work is that the thalamus possesses different classes of cortical-projecting neurons that participate in different parallel pathways originating in the retina.

On the other hand, some recent studies in the rodent visual thalamus seem to reveal greater complexity. For example, physiological evidence suggests that the average number of RGCs converging on a TC is approximately five, which is more than the maximum number reported in cat, ferret, or primates (Hong et al., 2014). Moreover, anatomical results suggest that the number of converging RGCs could be even greater (more than a dozen; Hammer et al., 2015). In rodents, attempts to classify TCs based on physiological properties seem to produce less-clear-cut categories than those described in other species (Grubb and Thompson, 2003; Gao et al., 2010). Although the spatial acuity in mouse visual system is lower than in carnivores and primates (Grubb and Thompson, 2003), rodent thalamic neurons are comparable in contrast sensitivity and center surround organization and exhibit at least as wide a range of selectivities for different visual features as other species (Piscopo et al., 2013). For all these reasons, rodents likely use their visual thalamus as other mammals do: to relay different channels of visual information from retina to cortex.

To study the synaptic basis for this parallel pathway organization, we acquired high-resolution EM images of a volume of about 67 million (i.e., 400 × 600 × 280) cubic microns (~100 trillion voxels) that included the full depth of the LGN. The ~100-TB dataset was then used to identify hundreds of RGC axons and the TCs they innervated. Our expectation was that a connectomic approach would reveal multiple sets of TCs, each with

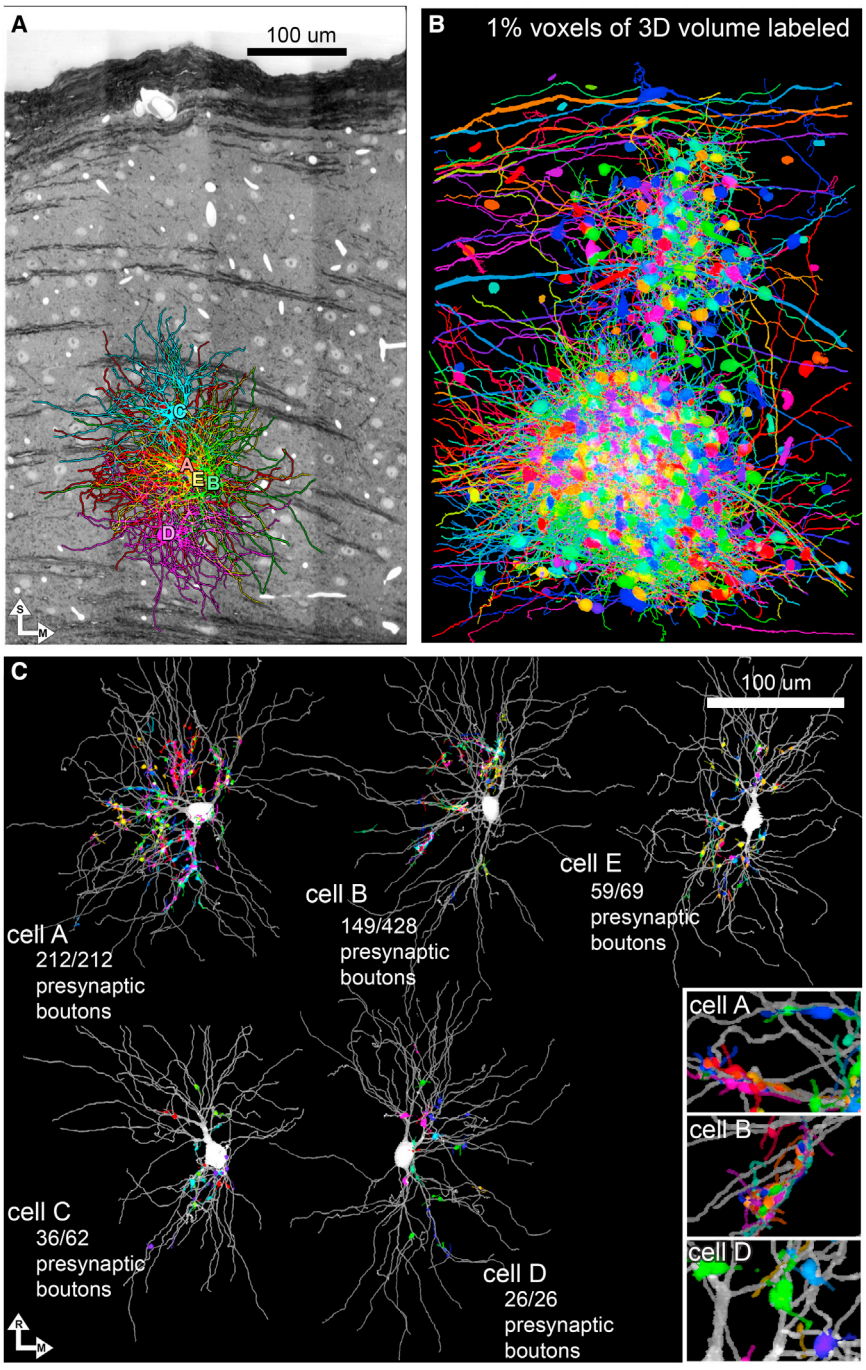


**Figure 1. A 0.07 mm$^3$ Volume of LGN Was Imaged in the Electron Microscope and a Network of >400 Neurons Reconstructed**

(A) Coronal section of LGN (Movie S1). Colors indicate seed cells A–D and cell E. Double arrow in this and subsequent images show the superficial (S), medial (M), or rostral (R) directions.

(B) Reconstructions of all the cells used for network analysis.

(C) Transverse view of the seed cells A–D and cell E with labeled presynaptic RGC boutons. Bouton color indicates which RGC axon gave rise to it. The presynaptic bouton fraction refers to the number of traced presynaptic RGC boutons relative to the total number of RGC boutons identified on that TC. Inset shows the different sizes of boutons on three seed cells: A's are large, B's are small, and D's are very large.

See also Figure S1.

its own characteristic cellular properties and RGC input type. The results, however, did not come out that way. Instead, we found a complicated pattern of different types of RGC axons forming intermixed synapses with a morphologically diverse population of TCs. The connectivity was not random, but not easily described by simple rules and difficult to divide into parallel pathways. These results raise the question of how mammalian neural networks implement even relatively straightforward physiological functions.

## RESULTS

### The LGN Volume

Using an automated tape-collecting microtome, we collected an ultrathin section library consisting of 10,000 sections (each 30 nm × ~1.5 mm × ~1.5 mm) from a P32 mouse LGN. One hundred trillion 4-nm wide pixels were imaged from this library using automated scanning EM (see Supplemental Experimental Procedures). The final aligned 3D image covers a 400-μm (mediolateral) × 600 μm (superficial-deep) × 280 μm (rostrocaudal) volume in the monocular region of the LGN (Figures 1A, S1A, and S1B; Movie S1). The superficial-deep dimension covers the entire depth of the LGN, including the optic tract (at the superficial limit). Automated detection of blood vessels revealed the LGN capillary bed (Figure S1C). Automated detection of lightly stained cell nuclei identified approximately 3,500 cell bodies within the volume, of which we believe ~3,000 are neuronal and the rest a subset of the glia (see Experimental Procedures; Figure S1D). Whereas we did some tracing at full resolution (Figure S1E), we found we could efficiently trace most processes with a dataset rendered four times down-sampled in the lateral dimensions. These tracings (4,937 objects) include 304 TCs (~10% of the total number in the volume) and 162 RGC axon segments (~5% of those in the volume). In total, ~1% of the imaged voxels were manually segmented (Figures 1B and S1F). The raw EM data and tracings can be accessed at https://software.rc.fas.harvard.edu/lichtman/LGN.

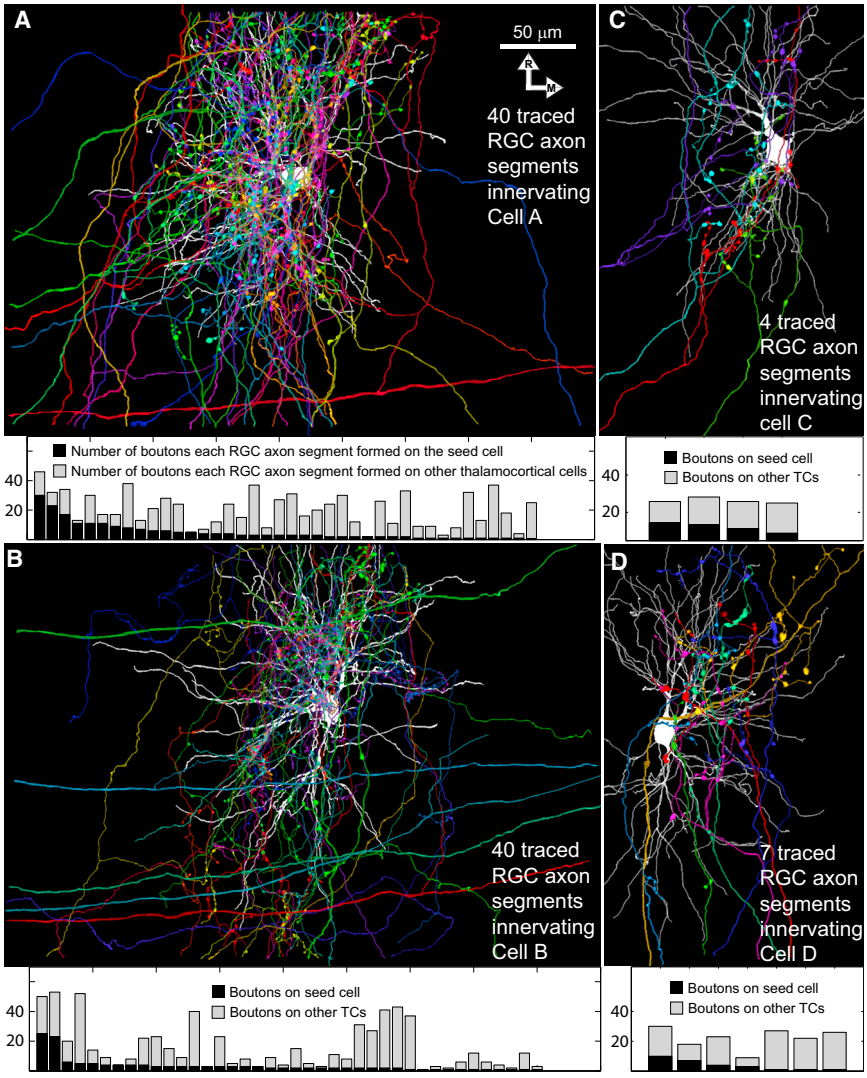


**Figure 2. The Structure and Synapses of Each Traced RGC Axon Innervating the Four Seed Cells**

(A) The RGC axon segments (each a separate color) that gave rise to all (212) boutons innervating seed TC A (white). Bar graph (also for B–D): the total number of boutons each axon formed on the seed cell (black) and the total number of boutons each axon formed elsewhere in the volume (gray) is shown. Most axons provided only a minority of their synaptic boutons to the seed cell.

(B) RGC axon segments innervating cell B.

(C) RGC axon segments innervating cell C.

(D) RGC axon segments innervating cell D.

See also Figure S2.

## Cellular Networks of the Mouse LGN

Below, we look at how RGCs (the LGN's driving input) distribute their axons among the TCs (the output neurons of the LGN). The approach we take is to reconstruct a "seed" TC as a starting point, identify RGC axons innervating it, and then identify the other TCs that are innervated by the same RGCs (Movie S2). RGC axons were identified by virtue of the distinctive light staining of their mitochondria (Guillery, 1969), allowing easy differentiation from cortical and inhibitory axons (Figures S1E, S1G, and S1H). Although RGC boutons innervated both TCs and local inhibitory neurons, we focused on the input to TCs. Local inhibitory neurons were distinguishable from TCs based on their own innervation of TCs (Famiglietti and Peters, 1972).

To begin, we chose two seed TCs that were adjacent (26 μm apart) and located in the middle of the volume (Figure 1A). These seed cells were chosen because their RGC synapses were structurally dissimilar in that the boutons on cell B were smaller and more clustered than the boutons on cell A (Figure 1C).

## Individual TCs Appear to Be Innervated by Many Retinal Ganglion Cell Axons at Postnatal Day 32

We reconstructed all the RGC axons that innervated cell A (Figure 2A). These axons provided 212 synaptic boutons and were concentrated on proximal dendrites. Thirty-seven of these axons were successfully traced to the edge of the volume, more than 100 μm from their nearest synapses with cell A. These axons exited the volume via large-caliber myelinated axonal shafts. Three additional axonal fragments could not be traced to the edge of the volume. We found that the RGC boutons on cell A formed synapses on dendritic shafts and on the small spines that grew adjacent to the boutons (Figure 7A). The number of boutons connecting individual traced axons to cell A ranged from 1 to 29 (Figure 2A). Many of the axons that formed only a few synapses with cell A established many synapses with other neurons in the volume (Figure 2A). Although most axons formed a small number of boutons with cell A (median = 3), more than half of the boutons (112) innervating the seed cell came from the seven axons that made the largest synaptic contributions (Figure 2A). We could find no obvious way to partition axons into subpopulations by connection number, rather there appeared to be a smooth continuum between a small number of axons that established many presynaptic boutons and many more axons that established few synaptic boutons.

We repeated this approach for cell B, whose RGC boutons had a different appearance. The small RGC boutons innervating cell B were clustered in dense synaptic glomeruli on the shaft of the dendrite or, more rarely, on spines (Figure 7A). We reconstructed all the RGC axons that innervated two particular synaptic glomeruli. Most of these (11/15) could be traced to the edge of the volume. Additionally, we partially reconstructed (i.e., traced at least >10 μm away from starting bouton) the retinal input to three other synaptic glomeruli. These tracings revealed 40

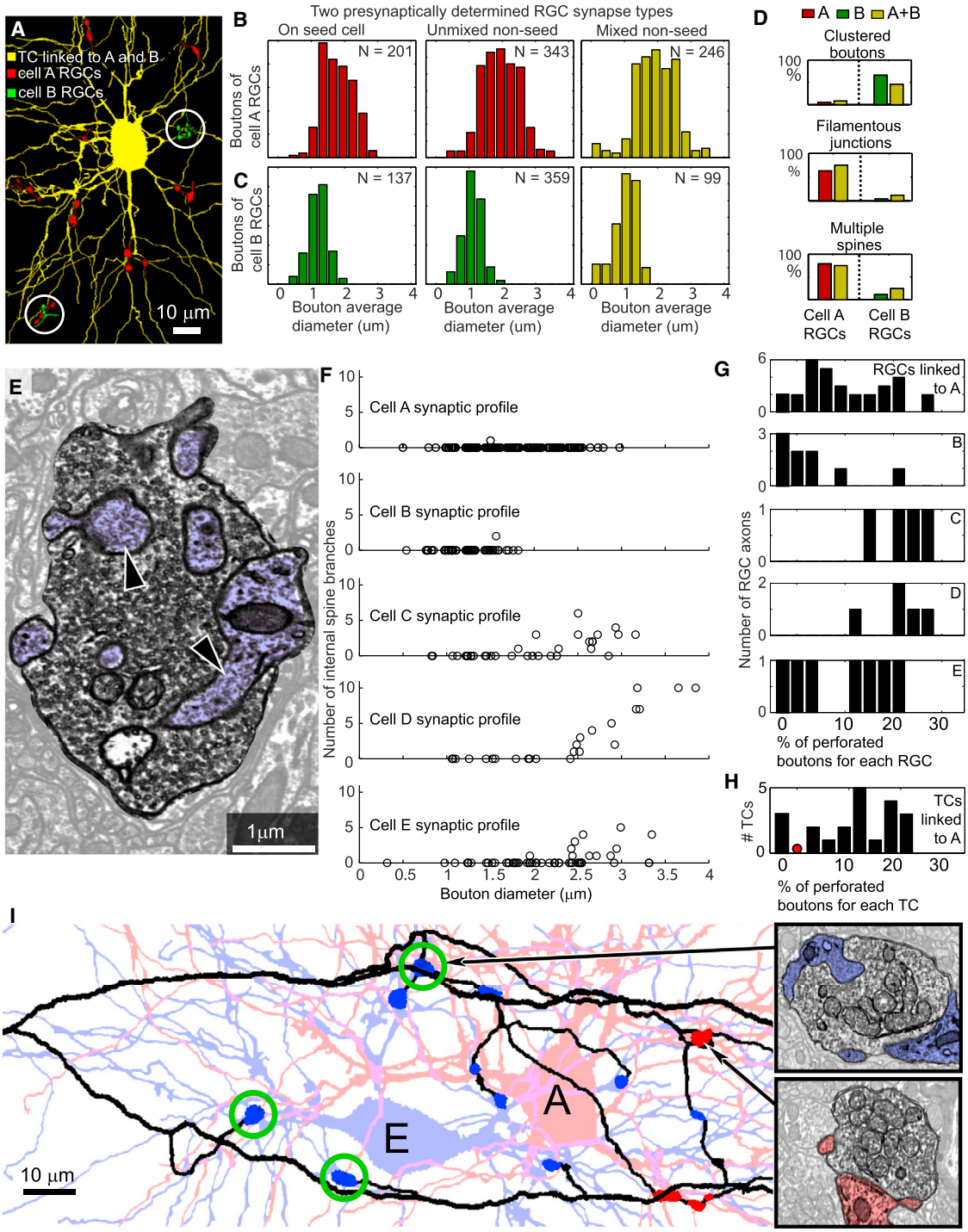


**Figure 3. Evidence for Both Pre- and Postsynaptic Influences on Synaptic Structure**

(A) A TC (yellow) is innervated by large boutons from RGC axons that also innervate cell A (red) and by small boutons from RGC axons that also innervate cell B (green; in circles).

(B) RGCs innervating cell A form large boutons on three groups of TCs. On cell A (left), 201 boutons, mean diameter = 1.8 μm, and 95% range = 1.0–2.5 μm. On other TCs (middle), 343 boutons, mean = 1.9 μm, and 95% range = 1.0–3.0 μm. On mixed TCs (right), 246 boutons, mean = 2.0 μm, and 95% range = 1.0–3.2 μm.

(C) RGCs innervating cell B form small boutons on three groups of TCs. On cell B (left), n = 137, mean = 1.2 μm, 95% range = 0.5–1.8 μm, and $p < 0.001$ (compared to B). On other TCs (middle), 359 boutons, mean = 1.1 μm, 95% range = 0.52–1.7 μm, and $p < 0.001$ (compared to B). On mixed TCs (right), 99 boutons, mean = 1.1 μm, range = 0.5–1.7 μm, and $p < 0.001$ (compared to B).

*(legend continued on next page)*

RGC axon segments that established 33% (140/428) of the RGC boutons innervating cell B. Two of these axon segments established substantially more synapses on cell B than the other axons (Figure 2B).

We were interested to learn how many different RGCs (as opposed to RGC axon segments) innervated each seed cell. The number of axons that were traced to the edge of the volume and that innervated seed cells A and B exceeds electrophysiological estimates of RGC convergence (1–6; Cleland et al., 1971; Mastronarde, 1992; Chen and Regehr, 2000; Jaubert-Miazza et al., 2005). Given that our reconstructions of the RGC axon arbors were limited to a 400 × 600 × 280 μm volume, it is likely that some of the entering axons are actually segments of the same RGC axon that branched outside the volume. However, in order for the 37 or >27 axons that reached the edge of the volume from cell A or cell B, respectively, to originate from, for example, just five RGCs, each RGC would have to form, on average, five large proximal branches before entering the EM volume and then travel more than 100 μm before converging on the same target cell. Optical imaging of mouse RGC axonal arbors shows that such axon branching can occur, but it is rare (Hong et al., 2014). The length of the axon segments therefore suggests that dozens of RGC axons converge on cells A and B—more than might have been expected. An anatomical study based on Brainbow fluorescence images has suggested that mouse TCs may be innervated by a dozen or more RGCs, which is in line with our estimate (Hammer et al., 2015).

## The Cohort of Axons Innervating One TC Also Innervates a Select Subset of Nearby TCs

Although each seed cell was linked to a large number of TCs via common RGC input, they were not linked to all of the surrounding TCs. We tested whether this arrangement was a sign of selectivity or occurred by chance. Of the 25 TCs within 50 μm of seed cell A (Figure S2), ten shared RGC input (i.e., were linked) to the seed cell. These ten postsynaptic cells were linked to the seed cell by 163 presynaptic boutons from 27 RGC axon segments. When we randomly distributed these 163 boutons (independently by Monte Carlo redistribution) onto all of the 25 nearby cells 100,000 times, most iterations linked all of the surrounding TCs to the seed cell (mean = 25.0 linked TCs; 95% range 24–25). The frequency of seeing ten or fewer linked cells was very small ($p < 0.0001$). This analysis treats each synaptic bouton independently, but it is possible that the contiguity of boutons of the same axon biases them toward innervating the same dendrite, thereby reducing the number of linked TCs. We therefore repeated our test for clustered connectivity using the binary measure of whether or not a given RGC formed any synapses with a given TC (39 connections in total). When we randomized which of the 25 nearby TCs each axon segment was connected to, we found an average of 19.9 linked TCs (95% range 17–23; 100,000 repetitions; $p < 0.0001$; Figures S2A–S2C). The RGC axons innervating cell A therefore connect with a smaller fraction of the nearby TCs than would have been predicted if innervation of TCs by RGC axons were random. We repeated these two analyses for seed cell B and found the same result: observed linked TCs = 8; bouton redistribution 95% range = 27–28 ($p < 0.001$); and binarized connections 95% range = 14–20 ($p < 0.001$; Figures S2D–S2F). This selectivity appears to support the idea of discrete parallel pathways associated with different cohorts of RGC axons (but see below).

Consistent with the idea of parallel pathways, the cohort of RGC axon segments innervating the two adjacent seed cells were almost completely different. Of the 79 RGCs segments traced from cells A and B that form 1,420 presynaptic boutons on TCs, there was only one RGC axon that innervated both cell A and cell B (it supplies one bouton to each).

Despite the lack of overlap in the innervation of the two seed cells, there was considerable mixing of the two cohorts of RGCs on other TCs. Of the 63 TCs linked to seed cell A and the 80 cells linked to seed cell B, 16 TCs were linked to both cells A and B (not counting the 11 TCs innervated by the RGC axon that innervated both seed cells; Figure S2G). Of the 66 TCs that receive input from more than one traced axon segment (the minimum requirement for detecting overlap), 24% shared RGC inputs with both seed cells A and B. The mixing of retinal input to these two sets of TCs is unexpected if the input to cells A and B reflected completely distinct channels of visual information passing through the thalamus.

## Synaptic Morphology Distinguishes Two Intrinsically Different RGC Types

Given that we observed different bouton properties (size and tendency to cluster) for the axons innervating the two seed cells (Figure 1C), we were interested to learn whether these differences were determined by the identities of the axons or by the identities of the postsynaptic cell being innervated. We first looked at the boutons on a TC that shared RGC inputs with both cells A and B. The two sets of axons innervated the mixed TC with boutons whose morphology matched that of the boutons the axons formed on their respective seed cells, resulting in a TC that received a mix of different types of synapses (Figure 3A). This observation raised the possibility that synaptic phenotype is set by axons rather than postsynaptic targets. To check the generality of this result, we analyzed the sizes of all the synaptic boutons of the traced RGC axons innervating cells

(D) Synaptic features of RGCs that innervate cell A (left side) and cell B (right side). Green bars, boutons on TCs linked to cell B; red bars, boutons on TCs that only share RGC input with cell A; yellow bars, boutons on TCs linked to both cells A and B.
(E) Perforated RGC bouton (highlighted) containing multiple internal TC dendritic spines (blue; arrows).
(F) A plot of the size and internal spine number for each RGC bouton innervating cells A–E. TCs exhibit different numbers of perforated boutons.
(G) Most RGC axons linked to seed cells A–E form both non-perforated and perforated boutons in the volume.
(H) The same axons that form only one perforated bouton total on cell A (of 212; red dot) form many perforated boutons on other TCs.
(I) Example axon that forms boutons on both cell A (red boutons) and cell E (blue boutons) but that only forms perforated boutons (green circles) on cell E. Insets show structure of perforated (top) and unperforated (bottom) boutons.
See also Figure S3.

A and B. We found that cell-A-associated RGCs formed the same distribution of large bouton sizes whether they were innervating cell A, other TCs, or mixed TCs (Figure 3B). The same consistency was observed for the small boutons formed by cell-B-associated RGCs (Figure 3C; see also Table S1). We observed the same axon-specific tendency in the clustering of synapses (Figure 3D). We thus conclude that there must be distinct types of RGCs innervating cell A and cell B and that the size and clustering tendency of these boutons is determined by the type of RGC axon rather than the type of postsynaptic TC.

Importantly, analysis of a subset of these axons revealed that the RGCs associated with the two seed cells were also strongly associated with different postsynaptic features (Figure 3D). Adjacent to 70% (of 43) of the sites where cell A RGCs formed synapses, the postsynaptic cytoplasm contained long endoplasmic reticulum (ER) assemblies, indicating the presence of a filamentous junction (Kadota and Kadota, 1979). Such filamentous junctions were only seen near 8% (of 224 boutons) of the cell B RGC synapses ($p < 0.001$). Likewise, 77% of the boutons of the RGC axons that innervated cell A contacted multiple TC spines, whereas only 18% of the boutons of the RGC axons innervating cell B contacted multiple spines ($p < 0.001$). These postsynaptic properties reflected the axon's identity in TCs that were innervated by both kinds of RGCs. Thus, RGC type appears to set both the pre- and postsynaptic structural features associated with its axon terminals (but see below).

### One RGC Axon Type Produces Synapses with Different Structures on Different Postsynaptic Cells

To learn whether there were other structurally distinct RGC types within the traced network, we examined the RGC inputs to several nearby TCs that did not share any RGC input with either cell A or B. A subset of these TCs was innervated by unusually large boutons that, similar to a type that was previously described (Rafols and Valverde, 1973; Spacek and Lieberman, 1974; El-Danaf et al., 2015), were perforated by multiple dendritic excrescences (TC spines; Figures 3E and 7A). These spines sometimes branched and occasionally passed all the way through the bouton. We observed single perforated boutons forming up to 45 active zones on ten internal spine branches from the same postsynaptic partner cell. Although rare, we found occasional perforated boutons that were presynaptic to multiple TCs.

We chose two TCs with perforated RGC inputs to be seed cells for further network tracing (cells C and D; Figures 1C, 2C, and 2D). We first quantified the differences in synaptic configurations (bouton size and internal spine number) for a subset of axons innervating cells A–D. The range of bouton sizes on cells C and D largely overlapped with the distribution of bouton sizes on cell A (Figure 3F). However, unlike cell A, the boutons on cells C and D appear to be of two types: the large perforated boutons just described and boutons that were not perforated by spines and generally not quite as large. The fraction of boutons with at least one internal spine was much higher on cells C and D (13/34 and 12/24) than the fraction on either cell A or B (1/202 and 1/66). Therefore, whereas boutons on cells A, C, and D can be categorized as large (relative to those on seed cell B), the distribution of synaptic profiles on cells C and D are distinguishable from cell A by taking into account the incidence of internal spines.

To learn whether the perforated boutons originated from a specific axon class, we analyzed the full arbors of nine axons innervating cell C (four) and cell D (five). We found that each of these axons bore some perforated boutons (11%–27% perforated; Figure 3G). Thus, all of the RGCs innervating cells C and D appear to be of the same structural type. Unexpectedly, when we did the same analysis for cell A, we found that most (29/31) of its innervating RGC axons also formed perforated boutons (Figure 3G). This result was surprising because only one internal spine was observed among the 212 synapses studied on cell A itself (Figure 3F). If each axon that innervated cell A randomly assigned which of its boutons were perforated, significantly more-perforated boutons would have been found on cell A (Monte Carlo median = 32; 95% range = 19–48; $p < 0.0001$). These results argue that the same axon behaves differently (in terms of perforated bouton formation) on different postsynaptic cells. To test this hypothesis further, we examined the synapses on the TC (cell E) that shared the most axons (ten) with seed cell A. We found that the frequency of perforated boutons on cell E (generated by axons that innervate both cell E and cell A) matched the distribution of inputs on cells C and D rather than the distribution observed on cell A. This result suggests that cell E is of the same type as seed cells C and D (despite sharing input with cell A). Moreover, cell E was not an exception; many of the TCs that shared RGC input with cell A perforated the boutons of those same RGC axons (Figures 3H and S3). Therefore, the presence or absence of perforated boutons reflects distinct synaptic behaviors of different TCs that are innervated by the same RGCs (!). Although we did observe small bouton RGCs sometimes clustering around elaborate spines (Figure 7A), we do not yet know whether this innervation also represents a distinct postsynaptic cell behavior. In summary, the same network exhibits synaptic properties set by axons (see previous section) and synaptic properties set by postsynaptic cells.

Aside from the presence of perforated boutons, cells C, D, and E were also different from cells A and B in that they were innervated by fewer boutons. However, the difference in number of boutons seemed to be offset by the number of release sites (active zones) associated with perforated boutons. Boutons on cell B (428) typically only formed one active zone, and boutons on cell A (212) typically formed several active zones. In contrast, of the boutons on cells C, D, and E (62, 26, and 52), many formed a dozen or more active zones. Across the five cells characterized then, we would expect the three distinct RGC input patterns to produce more-similar levels of RGC drive than would be predicted by looking only at the widely disparate number of boutons.

The perforated bouton TCs were also innervated by fewer RGC axons than the other seed cells. In the case of cell D, its entire complement of 26 presynaptic RGC boutons originated from only seven RGC segments (Figures 1C and 2D). Thus, among the postsynaptic neurons innervated by the same axons are subsets of neurons with distinctly different RGC bouton morphology, presynaptic bouton number, and RGC convergence. This suggests that different TCs process information from the same RGCs in different ways.

## Visualizing the LGN Network

To generate a connectivity map of all the traced RGC axons and TCs, we use a spring force model that positions neurons according to shared connectivity. In this model, every synaptic bouton (Figure S4A) acts as a spring so that pairs of neurons connected by more boutons will be pulled together with more force (Figure 4A; Movie S3). To remove the excessive influence of the seed cells on the spring force model (due to targeted tracing), we set the strength of connections of these cells to zero (see Figure S4A). In the resulting spring force distribution, the overall trend was for the RGCs associated with each seed cell to cluster together (Figures 4A, S4C, and S4D). Thus, RGCs with the same seed cell association are significantly biased toward innervating the same set of TCs. Indeed, 82% of pairs of RGCs that converge on the same non-seed TC also innervate the same seed cell (28% in random networks; 95% range 25%–30%; 428 convergences; $p < 0.0001$).

Clusters within the spring force model also had different synaptic characteristics. The bouton size and internal spine frequency of traced cells were concentrated in different parts of the spring force connectivity map (Figures 4B and 4C).

One potential cause of clustering is the spatial organization of the axons and TCs in the network. We therefore compared the somata positions of each of the seed cells and to the locations of the TCs synaptically linked to them (Figure 4D; Movie S4). The cohorts of TCs linked to seed cells C and D were largely non-overlapping in space (Figure 4E) and were also synaptically non-overlapping. In this case then, the lack of connectional mixing could be related to the different positions of the two sets of TCs. In contrast, there was considerable spatial overlap between the sets of TCs linked to cells A and B (Figure 4F). Despite this overlap, these cells still tended to be more associated with RGCs innervating one seed cell or the other as evident by their clustering in the network diagram (Figure 4A). By measuring the overlap of RGC axons and TC dendrites, we found that, even when RGC axons innervating cells A and B encountered the same TC dendrites, they formed synapses in a biased way. RGCs encountering a dendrite with a different seed cell preference (see Supplemental Experimental Procedures) were less likely to form synapses (11% of overlap prediction) than RGCs encountering dendrites with the same seed cell preference (130% of overlap prediction; bootstrap difference between groups; 95% range = −42%–40%; $p < 0.001$). Anatomical segregation, therefore, cannot fully explain the clustered patterns of connectivity we observed in the spring force distribution.

To more comprehensively compare the position and connectivity of neurons, we developed an objective means of subdividing the network into subgroups (“clades”). We used the spring force model (minus the seed cells) to identify outlier connections (the longest edges) and then removed these edges one at a time. This procedure resulted in the erosion of the fully connected network into progressively smaller disconnected subnetworks (Movie S3). We visualized this progressive ungrouping in a dendrogram (Figure 4G). The groupings generated by this network erosion are similar to what we observed when we partitioned the graph using spectral clustering (Ng et al., 2002; Figure S5A) and are, with some notable differences, consistent with the clustering of RGCs according to seed cell association (Figure 4G, left side). For example, eroding the network into the first six clades produced four cohorts of TCs associated with the four seed cells but also generated two additional clades (Figures 4G and 4H). The cells associated with seed cell B were divided into three different groups: two consisting only of cell-B-associated neurons (green and white clade) and a third group that was composed of both cell-B- and cell-A-associated neurons (blue clade; Figures 4G and 4H).

We investigated how these six subnetworks were spatially organized in the LGN (Figures 4I, S5B, and S5C). Five of the six clades did have a spatial bias as revealed by a predominant location (i.e., hue) of the RGCs and TC somata in each group (RGC location was assigned by the mean position of its boutons). In contrast, the green clade was distributed more evenly throughout the volume. This wider distribution is evident by looking at the positions of the TC cell bodies (Figures 4J, S5D–S5E, and S5H), the spread of the RGC axon arbors (Figures 4K, S5F, S5G, and S5I), and in the position of the synapses between RGCs and TCs from the green clade (Figure 4L). The LGN, therefore, possesses some synaptically connected networks of neurons that are spatially organized into partially non-overlapping regions. Intercalated within this spatially organized network, however, we also see another subnetwork (the green clade) that is segregated from the other clades by synaptic preference rather than by location.

## Dendritic Morphology Does Not Appear to Dictate Connectivity

Given that a number of studies associate the electrophysiological types of TCs to different dendritic morphologies (Friedlander et al., 1981; Stanford et al., 1983), we wanted to know whether the dendritic geometry of TCs correlated with their connectivity in this network. Using two automated approaches (principal component and Sholl analyses), we characterized the shapes of TC dendritic arbors. Both methods looked at the number of orientations across which dendritic arbors extended. We found a variety of cell morphologies in the traced network: biconical cells (arbors oriented in the rostrocaudal, dimension); saucer-shaped cells (flattened in the superficial-deep axis); and cells that extended equally in all dimensions (Figures 5A and 5B).

None of the morphological measures we tested appeared to be strong predictors of network connectivity (Figure 5C). One measure (Sholl) showed that biconical shape weakly correlated with position in the dendrogram (Figure 5C). However, as seen by overlaying TC shape on the spring force diagram, neurons with different morphologies are found in each region of the network and were often innervated by the same RGC axons (Figures 5D and 5E). For example, both large- and small-bouton RGCs innervated biconical cells. We thus conclude that cell shape per se is not a strong determinant of which group of RGC axons innervate a TC neuron. Other potential anatomical markers of cell type (cell body size, filamentous junctions, and laminar bodies) yielded similarly mixed distributions (Figures S6A–S6F).

## Dendritic Subnetworks?

Looking at network connectivity at a subcellular level revealed organization that was not visible when cells are treated as single

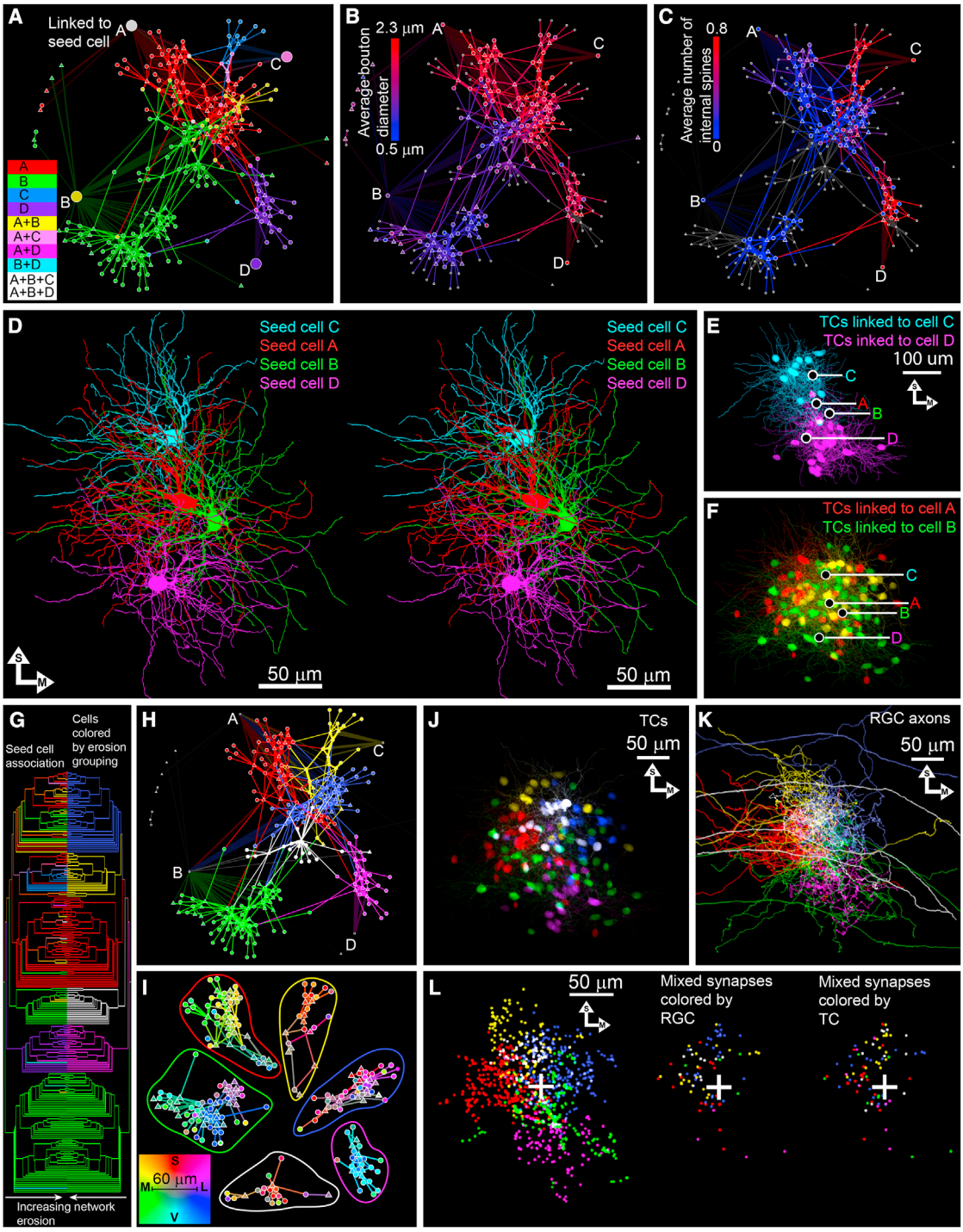


**Figure 4. A Spring Force Connectivity Map Reveals a Synaptically Interconnected LGN Network with Both Spatial and Non-spatial Organization**

(A) Spring model of synaptically connected (lines) RGCs (triangles) and TCs (circles) forms clusters that correspond to their seed cell association. The color-coded legend identifies RGCs based on seed cell innervation. The color of each TC reflects the seed cells with which the TC shares RGC input. Spring strength (indicated by line thickness) reflects the number of boutons connecting each RGC to each TC. Seed cells (A–D) are excluded from influencing the cell distribution (springs set to 0). See also Figure S4.

(B) Segregation of RGCs and TCs with large average bouton diameters (red) from small bouton diameters (blue). Cells with fewer than five identified boutons are gray.

(C) Non-random distribution of perforated boutons. Cells with fewer than ten identified boutons are gray.

*(legend continued on next page)*

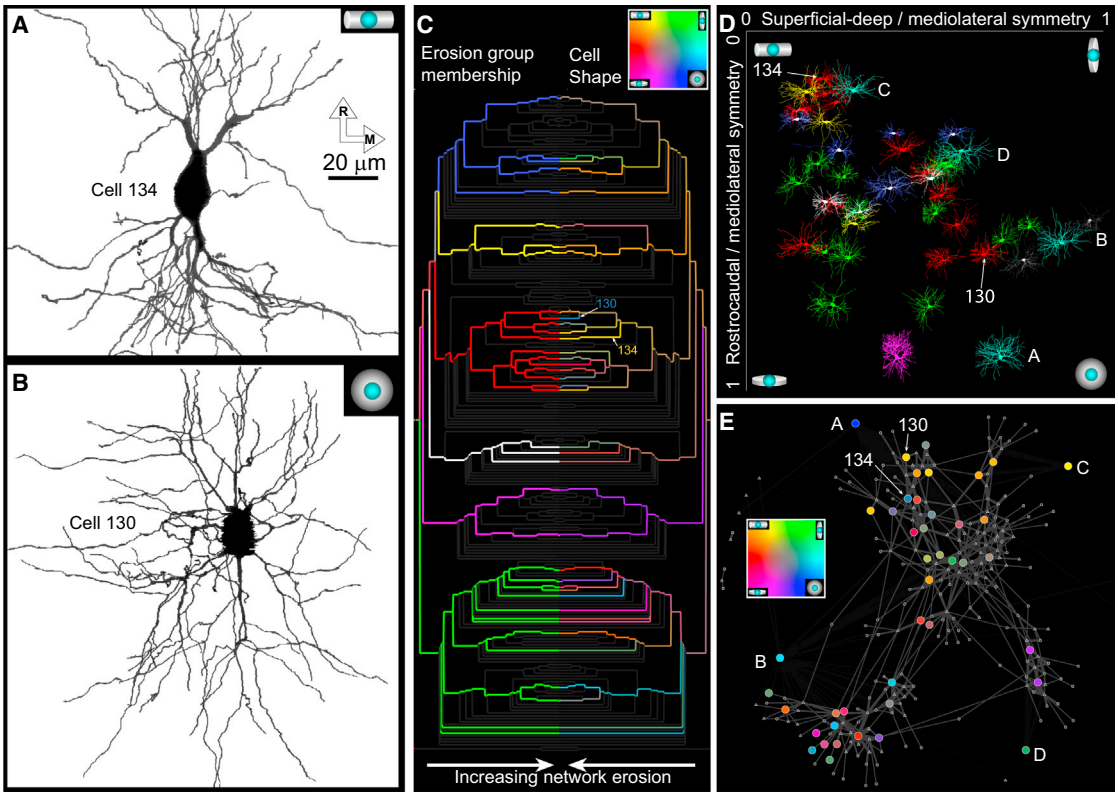


**Figure 5. TCs with Different Dendritic Arbor Shapes Found throughout the Network**

(A) Example of a biconical dendritic arbor (cell 134). Inset shows biconical arbor icon.

(B) Example of a symmetric dendritic arbor (cell 130). Inset shows symmetric arbor icon.

(C) Different arbor shapes are found in the same subnetworks of the dendrogram. Left side shows erosion group membership (colors from Figure 4H) of morphologically characterized TCs. Right side shows shape of TCs based on Sholl analysis. Key colors indicate biconical, flattened, or radially symmetric arbors. Cells 134 and 130 from (A) and (B) (arrows) are adjacent in the dendrogram. For 39 TCs, correlation coefficient (r) between similarity of shape and connectivity is 0.15. For randomly assigned cell shape, r = 0, 95% range = −0.09–0.10, and p = 0.008, adjusted for multiple tests.

(D) Plot of TC arbor shape with TCs colored according to erosion grouping (except the four seed cells labeled cyan).

(E) Spring force diagram with morphologically characterized TCs colored according to shape (as in C).

See also Figure S6.

nodes in the network. For example, the inputs associated with the three clades of RGC axons innervating cell A (blue, yellow, and red; Figure 6A) tend to innervate different regions of the dendritic arbor (Figure 6B). To some degree, this regionalization reflects the different positions of the RGC axons from these three clades (Figure 6C).

On cell B, however, we saw a more-fine-grained dendritic organization of RGC input and one that was less easy to ascribe simply to the positions of RGC axonal projections. On cell B, multiple RGC axons glom onto a single dendritic site by forming a densely spaced cluster of synapses (as described previously by Famiglietti and Peters, 1972). We noticed, however, that

(D) Relative positions and dendritic overlap of seed cells A–D (stereo pair for crossed eye viewing; see also Movie S4).

(E) Non-overlap of the TCs linked to cells C (cyan) and D (purple). Colored circles indicate seed cell positions (also in F).

(F) Spatial overlap of TCs linked to cell A (red), cell B (green), and both A and B (yellow).

(G) Network erosion dendrogram (seed cells excluded) used to identify network substructure (see also Movie S3). Colors indicate seed cell association (left; see Figure 4A for color scheme) or the first six erosion groupings (right; see Movie S3, s 14).

(H) Spring force diagram colored according to the erosion groupings from (G) (right side).

(I) Relative positions of TCs and RGCs (see key) divided into the six groups shown in (H). The green group has the widest spatial distribution of any subnetwork and overlaps with several other subnetworks.

(J) Spatial mixing and segregation of erosion groupings (color from H) of synaptically related TCs. See also Figure S5.

(K) Spatial mixing and segregation of erosion groupings (color from H) of synaptically related RGCs.

(L) Spatial mixing and segregation of synapses within and between erosion groupings (color from H) of RGCs and TCs. (Left) Synapses between RGCs and TCs from the same group are shown. (Middle and right) Greater mixing of synapses formed between RGCs and TCs from different groups is shown (colored according to the RGC [middle] or TC [right]). White cross indicates center of traced volume.

See also Figures S4 and S5.

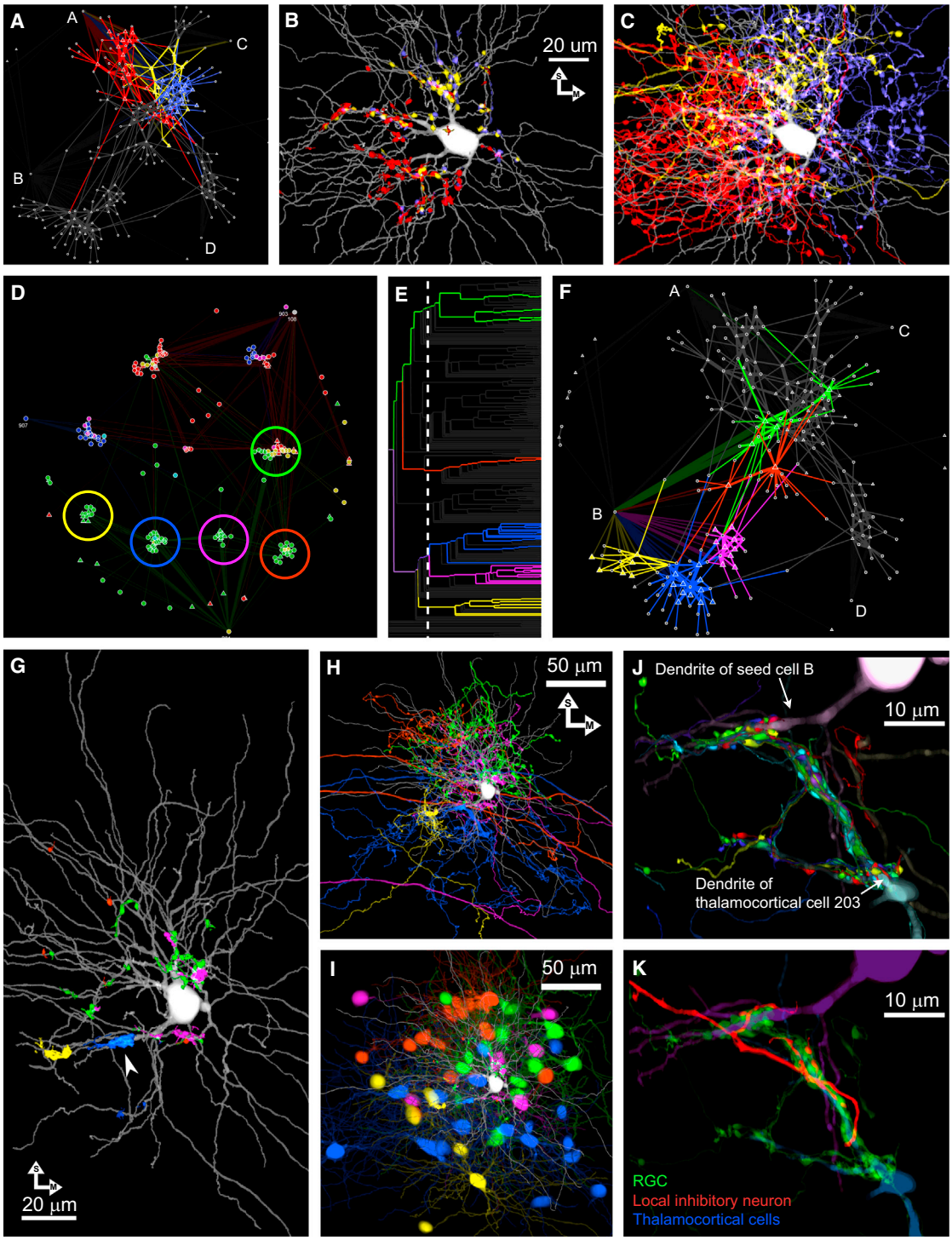


**Figure 6. Different Subnetworks of RGC Axons Innervate Different Parts of Individual TC Dendritic Arbors**

(A) Spring force distribution of the three groups of RGCs that innervate cell A (colors from Figure 4H).

(B) Non-uniform dendritic distribution of different groups of RGC synapses (colored as A and Figure 4H) on cell A.

(C) Axon arbors (colored as A) of the different RGC groupings that generate the bouton distribution in (B).

(D) Network erosion breaking the axons innervating cell B into five groups. Circles indicate the colors used for these groups in (E)–(G). See Movie S3, at 18 s.

(E) Erosion dendrogram showing the five RGC subgroups linked to seed cell B. Dotted line indicates the stage of erosion that defines the five groups in (D).

(F) Spring force distribution of the five clusters of RGCs that innervate cell B.

*(legend continued on next page)*

different sets of axons were associated with each glomeruli on cell B. In an attempt to learn whether there was any significance to which particular axons comprised each glomerular set, we explored the grouping identities in the network dendrogram (Figure 4G). By further erosion of the dendrogram, we divided the RGCs innervating cell B into five distinct groups (Figures 6D–6F; Movie S3). Surprisingly, the sets of axons associated with each group corresponded to different glomeruli on cell B's dendritic arbor (Figure 6G). Thus, different dendrites of one TC are synaptically segregated into different parts of the network. In contrast to cell A, the network segregation of boutons on the dendritic arbor of cell B occurred on a very fine scale relative to wide distribution of the RGCs and TCs they were linked to (Figures 6G–6I; Movie S5).

Examination of the microstructure of the RGC axons provided an explanation for this segregation. We found that the axons innervating a glomerulus of one TC cell dendrite organized as a fasciculated bundle and stuck together long enough to jump onto nearby dendrites of a different TC (Figures 6J and S7A–S7F; Movie S6). This fasciculation allows recapitulation of essentially the same input pattern to different glomeruli of dendrites from different TCs. In this way, a local synaptic motif generates a network motif. There may be other synaptic motifs in the LGN that similarly coordinate inputs onto dendrites of different TCs (Figures S7G and S7H). We do not, at present, understand how this organization is used in a functional sense, but it is interesting that such a transneuronal duplication of inputs also extends to inhibitory inputs from local interneurons (Figure 6K). These local network structures therefore appear to organize connectivity in the visual system at a finer scale than would be predicted from the superposition of the axonal arbors of RGCs with the dendritic arbors of TCs.

## DISCUSSION

### Bottom Up Approach to Mapping Neural Networks

In this work, we analyze the network that connects retinal axons and cortical-projecting neurons in mouse visual thalamus by acquiring a large amount of EM data from one specimen. Typically, network understanding has come from combining smaller amounts of information from many specimens. But that approach omits several kinds of information such as variation within a class of neurons and the organization of axons relative to other axons of the same type (Morgan and Lichtman, 2013). Here, we obtained connectivity of many axons and their targets located in the same region without regard to the explicit type of RGC axon or type of TC. Groupings of cells emerged were based strictly on the discovered properties of the circuit.

The traced cells shared morphological properties with previously published RGCs and TCs. For example, synapses were divided into four ultrastructural types: large bouton non-perforated; large bouton perforated; small bouton shaft glomerulus; and small bouton spine glomerulus (Figure 7A; Rafols and Valverde, 1973; Wilson et al., 1984; Spacek and Lieberman, 1974; Lieberman, 1974). In addition, the observed connectivity differences between large- and small-bouton RGCs parallel differences between Y and X RGCs (respectively) in cat (Sur et al., 1987; Yeh et al., 2003). Likewise, the biconical, saucer-shaped, and spherical TC dendritic arbors we describe have previously been seen in rodents (Krahe et al., 2011; Ling et al., 2012). In much of the previous literature, these structural features were argued to reflect functionally distinct types of neurons.

The conclusions we reached, however, diverged from previous studies. When we grouped cells by their connectivity, we were unable to divide TC cells into separate types with homogeneous structural properties. Moreover, we found large numbers and different types of RGC axons innervating single TCs. In contrast, in primates, LGN sub-lamina receives distinctly different types of RGC inputs (Leventhal et al., 1981) and few RGC axons are thought to innervate each cell (Lee et al., 1983).

### Fuzzy Sets of Neurons in the LGN

If there was any part of the CNS that one might expect to see well-ordered segregation between parallel pathways, it would be in the LGN. Instead, this network consists of converging and diverging pathways in which various cell properties could be found in every combination (Figure 7B). This result seems to be in accord with physiological results showing "only weak preferences" of mouse TCs for particular spatiotemporal visual features (Gao et al., 2010). Using fuzzy k-means clustering in mouse thalamus, Piscopo et al. (2013) defined six functionally different groups of TCs. We think fuzzy clustering may be more than just an analytical strategy and reflects the actual synaptic organization of the LGN.

In fuzzy sets, individuals are assigned degrees of membership in multiple groups (Zadeh, 1965). This organization contrasts with the classical view of sets in which elements either belong or don't belong to a set. Fuzzy sets describe the network we reconstructed because cells associated by connectivity with one cluster were often also associated with another cluster, i.e., had membership in more than one group (Figure 4). We also observed fuzziness when we classified TCs according to their dendritic geometry versus their network connections (Figure 5). The cleanest division in this data were two distinct populations of RGCs axons, those with large versus small boutons. But the connectivity distinctions between these two types of RGCs were fuzzy: RGC axons from both populations sometimes

(G) The five groups of RGCs (D) innervate largely non-overlapping glomeruli within cell B's dendritic arbor. Each color represents a set of axons (orange, 2 axons; green, 4; yellow, 6; purple, 9; and blue, 11; see F). The arrow points to the glomerulus shown in (J).
(H) The RGCs of each of the five groups are distributed over a large area relative to their innervation of cell B (Movie S5).
(I) The TCs belonging to each group are distributed over a large area relative to the bouton clusters in (G).
(J) RGC fascicles that jump from one dendrite to another help explain the subneuronal network organization shown in (G). Many RGC axons forming a synaptic glomerulus on cell B (the magenta dendrite of seed cell B) travel together to a nearby dendrite of a different TC (cyan dendrite of cell 203).
(K) A local inhibitory neuron (red) mirrors RGC innervation (green) of two glomeruli on different TCs (magenta and cyan; see J).
See also Figure S7.

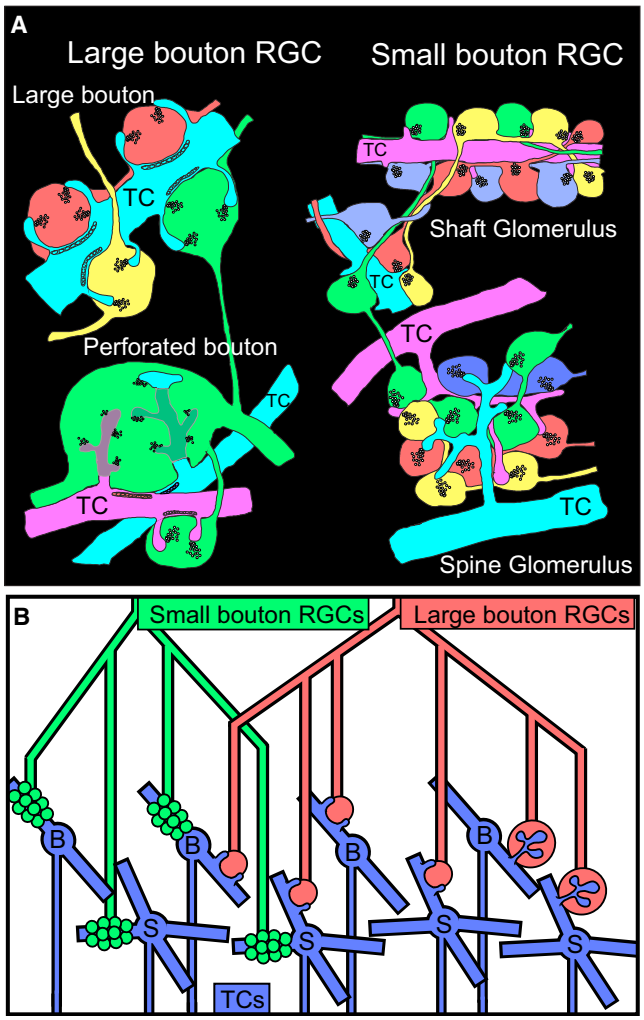


**Figure 7. Summary of Synaptic and Network Motifs in this Region of the LGN**

(A) Four synaptic configurations generated by two RGC types in the traced LGN network.

(B) Variations in the properties of RGCs (small or large synaptic boutons) and TCs ("B," biconical arbor; "S," symmetric arbor) produce many distinct TC input patterns (eight combinations shown here). All of these input patterns were found within the same interconnected network. Synaptic configurations (from left to right) refer to shaft glomerular, large bouton with external spine, and perforated bouton synapses. Please note that we find considerably more axons converging on each TC than the one or two shown here.

co-innervated the same TCs. TCs could therefore be said to belong, with varying degrees of membership, to sets of TCs innervated by large- or small-bouton RGC axons. The logic of the LGN wiring therefore is fuzzy.

## Fuzziness as Noise, Complexity, or Diversity

Why is there fuzziness in this network? One possibility is that connectivity in biological networks is sloppy in the sense that different types of RGCs occasionally innervate the same TC by accident. In a classic serial EM study of the cat LGN, Hamos et al. (1987) invoked this idea to explain why an X-type RGC formed a small connection with a Y-type TC. In our network, we observed many weak connections between RGCs and TCs that were far apart in the network diagram consistent with there being some probability that any RGC will form a synapse with any overlapping TC independent of type. However, sloppy wiring is unlikely to explain all the intermixing. For example, innervation by both large- and small-bouton RGC axons was found on many TCs, but the small-bouton RGCs supplying this innervation were not a random subset, rather they all also innervated the same glomerulus on one of the seed cells (Figure 6F).

Another possibility is that the apparent fuzziness is an artifact based on incomplete sampling of the actual network. Although we studied 154 TCs, excepting the seed cells, we annotated only a small fraction of the retinal synapses on each TC. Is it possible that there is a strictly determined connectivity pattern present in the LGN, but our sampling was too sparse to detect it? Could, for instance, there be a particular type of TC that always gets half of its inputs from large-bouton RGCs and half of its inputs from small-bouton RGCs? Mastronarde (1992), using physiological measures in cat LGN, classified as a type the TCs that received input from both X- and Y-type RGCs. Perhaps additional reconstruction in the mouse LGN will show that the variety of intermixing arrangements fall into distinct classes. This seems unlikely, however, because, across virtually all the parameters we analyzed, fuzziness was commonplace: every combination of RGC input types was found to innervate different TCs, and none of these combinations strongly correlated with the particular dendritic geometry nor the intracellular histological properties of the innervated TCs (Figures 5, 7, and S6). Finding such a variety of connection motifs may have a more-parsimonious explanation (below).

Finally, might fuzziness be the result of an adaptive mechanism to generate diversity? In the traced network, two morphologically distinct RGC types were mixed together to form eight different TC input patterns (Figure 7B) and different degrees of convergence. We would expect such a range of patterns could produce TC responses that vary in their temporal properties, receptive field sizes, and receptive field shapes. Such mixing should produce neurons with a wider range of spatial and temporal response properties than present in RGCs (Alonso et al., 2006; Martinez et al., 2014; Marshel et al., 2012). The idea of an ordered peripheral sensory network that gives rise to diverse combinations of connectivity in the next stage of processing has also been described in *Drosophila* where anatomically and functionally well-defined olfactory glomeruli generate a more-mixed and random input organization in the mushroom body (Caron et al., 2013).

If fuzziness is an adaptive advantage, how might it arise? The properties of neurons in the adult LGN are shaped during development by activity-dependent synaptic reorganization (Sretavan et al., 1988; Chen and Regehr, 2000; Tavazoie and Reid, 2000; Hong et al., 2014). The network structure we have observed may be a reflection of these activity-dependent processes. If the thalamus reorganizes in a way that is analogous to the developing rodent neuromuscular system, then in postnatal life, the wiring diagram is not simply "fine-tuned" to modify a nearly

perfect intrinsic pattern but rather undergoes a profound and pervasive network rebuilding (Tapia et al., 2012). If thalamic connectivity was based on experience per se, then it would not be surprising that the same postsynaptic cell might be co-innervated by diverse inputs that have some correlations during the experience-dependent phase of network development.

### Neurons as Types or Individuals?

It is universally accepted that neurons can be categorized into distinct types with distinct functions. We therefore expected to classify cells into types from the bottom up by describing morphological characteristics and connectivity of each of the cells in the network. However, we found that individual neurons had membership in multiple fuzzy sets, and our attempts at classification failed. It was not that all the TCs are alike, but there was no single criterion that could be used to consistently divide the population into subgroups whose members were homogeneous. Instead, each cell seemed to have unique attributes related to the assignment of many largely independent parameters. To us, the situation for single cells in the thalamus seems analogous to the classification of human individuals by a large number of partially independent criteria (e.g., language, height, gender, occupation, etc.). It may be unproductive, therefore, to talk about how many types of cells exist when every combination of every attribute is possible, just as the case with people. This view is more consistent with the behavior of neuronal networks as complex biological systems. This is not to say that there are not different types of cells: no one would argue that local inhibitory neurons and excitatory neurons are not distinct types. However, we do not yet know where to draw the line, or whether a clear line can be drawn, between divisions of fundamentally distinct cell classes, reliably identifiable subtypes, and the diverse behaviors of a given type of neuron.

### Networks of Neurons or Networks of Synapses?

Despite our difficulty grouping neurons, we found we could clump individual dendrites of multiple neurons into groups (Figure 6). Dendrites of different TCs could have nearly identical RGC inputs by virtue of the local fasciculation of whole sets of RGC axons that crossed from one dendrite to another. As a consequence, different dendrites of the same cell participated in different parts of the network. Functional modeling of response properties then might be best achieved if each dendrite is a separate node whose activity is compared to that of other dendrites via connection to a central cell body node (Poirazi et al., 2003). Because the local fasciculated axons also included an inhibitory input, it is possible that a cell could switch its properties by turning on or off individual dendrites.

### Lessons Learned

One of the goals of this project was to generate a high-resolution dataset that covered enough volume that we could bridge two types of inquiry: cellular structure and network structure. When we did so, we found that the common assumption that neural pathways would be well defined (often employed when cell properties are being investigated) and the common assumption of homogeneous cell properties (often employed when networks are being investigated) were not borne out. Instead, we observed a cellular network whose complex organization would have been difficult to infer from less-direct inquiry. The addition of more cells and cell properties to the traced network had a multiplicative effect on the complexity we uncovered; at least at this point we do not believe we have reached a point of diminishing returns where more tracing would simply reveal more of the same information. We have made the LGN dataset publicly available (https://software.rc.fas.harvard.edu/lichtman/LGN) and intend to continue investigating the network embedded in this digital tissue.

## EXPERIMENTAL PROCEDURES

All animals were handled according to protocols approved by the Institutional Animal Care and Use Committee at Harvard University. Detailed protocols are available in the Supplemental Experimental Procedures.

A P32 C57-Blk6 mouse was perfused with 2%–2% PFA/glutaraldehyde. The brain was post-fixed and cut into 300-μm vibratome sections. A slice passing through the middle of the LGN was selected for study and then stained with OTO (2% osmium tetroxide, 0.1% thiocarbohydrazide, and 2% osmium tetroxide) and 4% uranyl acetate. The LGN was then dehydrated using acetonitrile and embedded in Araldite 502 resin. Ultrathin sections were cut using ATUM (Hayworth et al., 2014; Kasthuri et al., 2015) and post-stained with 3% lead citrate. Prior to imaging, sections were plasma etched to remove contaminants and enhance contrast.

Images were acquired using custom imaging software (WaferMapper; Hayworth et al., 2014; https://software.rc.fas.harvard.edu/lichtman/LGN), driving a Zeiss Merlin SEM with a Fibics scan generator. Images were stitched and aligned using a signal-whitening Fourier transform (SWiFT) method. This method uses the low-resolution section alignment that was generated during the initial mapping of the section series as its starting point. It then steps through increasingly higher-resolution levels, each time aligning the images to a three-dimensional estimate of the local volume extrapolated from previous lower-resolution iterations. All tracing of synaptic connectivity was done manually in VAST by the authors. Tracings of the dendritic arbor morphology of some TCs were done by volunteers. The p values for comparisons between two groups were determined using Mann-Whitney U tests unless otherwise stated. For morphological analysis of axons and dendrites, we used a shortest-path algorithm to convert volumetric tracings into skeleton representations.

To test for a relationship between connectivity and arbor shape, we first measured the similarity between the shapes of every potential pairing of morphologically characterized TCs. We then found the stage in synaptic erosion at which each pairing of cells split apart. We then tested for a correlation between the two numbers to see whether cells with similar morphologies stuck together longer as the network was pulled apart.

## SUPPLEMENTAL INFORMATION

Supplemental Information includes Supplemental Experimental Procedures, seven figures, one table, and six movies and can be found with this article online at http://dx.doi.org/10.1016/j.cell.2016.02.033.

## AUTHOR CONTRIBUTIONS

J.L.M. and J.W.L. designed the experiment. J.L.M. acquired the data. A.W.W. aligned the images. D.R.B. developed manual segmentation software. J.L.M. and D.R.B. segmented the dataset with help from student volunteers (see Acknowledgments). J.L.M. rendered and analyzed the segmentations and developed the related software. J.L.M. and J.W.L. wrote the manuscript.

## ACKNOWLEDGMENTS

We gratefully acknowledge support from the NIH/NINDS (1DP2OD006514-01, TR01 1R01NS076467-01, and 1U01NS090449-01), IARPA via DoI/IBC

(D16PC00002), Conte (1P50MH094271-01), MURI Army Research Office (contract no. W911NF1210594 and IIS-1447786), NSF (OIA-1125087 and IIS-1110955), the Human Frontier Science Program (RGP0051/2014), and the NIH and NIGMS via the National Center for Multiscale Modeling of Biological Systems (P41GM10371). We are grateful to Linda Xu, Jacob Wasag, Aidan Piper, Seaun Yoo, Shana Attar, Katherine Mateos, Abigail Orlando, Anne Crosby, Kyla Cordrey, Allan Ordonez, and Marquise Bartley, who helped segment the data. We are grateful to James Cuff and his expert staff at Harvard Research Computing for data management, to Hanspeter Pfister and his lab members for help with image storage and alignment, and to Richard Schalek for management and troubleshooting of the EM hardware. We are also grateful to R. Clay Reid, who was involved in the initial planning and support.

Received: October 2, 2015
Revised: December 11, 2015
Accepted: February 12, 2016
Published: March 24, 2016

## REFERENCES

Alonso, J.-M., Yeh, C.-I., Weng, C., and Stoelzel, C. (2006). Retinogeniculate connections: A balancing act between connection specificity and receptive field diversity. Prog. Brain Res. *154*, 3–13.

Caron, S.J.C., Ruta, V., Abbott, L.F., and Axel, R. (2013). Random convergence of olfactory inputs in the Drosophila mushroom body. Nature *497*, 113–117.

Chen, C., and Regehr, W.G. (2000). Developmental remodeling of the retinogeniculate synapse. Neuron *28*, 955–966.

Cleland, B.G., Dubin, M.W., and Levick, W.R. (1971). Simultaneous recording of input and output of lateral geniculate neurones. Nat. New Biol. *231*, 191–192.

Cruz-Martín, A., El-Danaf, R.N., Osakada, F., Sriram, B., Dhande, O.S., Nguyen, P.L., Callaway, E.M., Ghosh, A., and Huberman, A.D. (2014). A dedicated circuit links direction-selective retinal ganglion cells to the primary visual cortex. Nature *507*, 358–361.

Dhande, O.S., and Huberman, A.D. (2014). Retinal ganglion cell maps in the brain: implications for visual processing. Curr. Opin. Neurobiol. *24*, 133–142.

El-Danaf, R.N., Krahe, T.E., Dilger, E.K., Bickford, M.E., Fox, M.A., and Guido, W. (2015). Developmental remodeling of relay cells in the dorsal lateral geniculate nucleus in the absence of retinal input. Neural Dev. *10*, 19.

Famiglietti, E.V., and Peters, A. (1972). The synaptic glomerulus and the intrinsic neuron in the dorsal lateral geniculate nucleus of the cat. J. Comp. Neurol. *144*, 285–333.

Friedlander, M.J., Lin, C.S., Stanford, L.R., and Sherman, S.M. (1981). Morphology of functionally identified neurons in lateral geniculate nucleus of the cat. J. Neurophysiol. *46*, 80–129.

Gao, E., DeAngelis, G.C., and Burkhalter, A. (2010). Parallel input channels to mouse primary visual cortex. J. Neurosci. *30*, 5912–5926.

Grubb, M.S., and Thompson, I.D. (2003). Quantitative characterization of visual response properties in the mouse dorsal lateral geniculate nucleus. J. Neurophysiol. *90*, 3594–3607.

Guillery, R.W. (1969). The organization of synaptic interconnections in the laminae of the dorsal lateral geniculate nucleus of the cat. Z. Zellforsch. Mikrosk. Anat. *96*, 1–38.

Hammer, S., Monavarfeshani, A., Lemon, T., Su, J., and Fox, M.A. (2015). Multiple retinal axons converge onto relay cells in the adult mouse thalamus. Cell Rep. *12*, 1575–1583.

Hamos, J.E., Van Horn, S.C., Raczkowski, D., and Sherman, S.M. (1987). Synaptic circuits involving an individual retinogeniculate axon in the cat. J. Comp. Neurol. *259*, 165–192.

Hayworth, K.J., Morgan, J.L., Schalek, R., Berger, D.R., Hildebrand, D.G.C., and Lichtman, J.W. (2014). Imaging ATUM ultrathin section libraries with WaferMapper: a multi-scale approach to EM reconstruction of neural circuits. Front. Neural Circuits *8*, 68.

Hong, Y.K., Park, S., Litvina, E.Y., Morales, J., Sanes, J.R., and Chen, C. (2014). Refinement of the retinogeniculate synapse by bouton clustering. Neuron *84*, 332–339.

Jaubert-Miazza, L., Green, E., Lo, F.-S., Bui, K., Mills, J., and Guido, W. (2005). Structural and functional composition of the developing retinogeniculate pathway in the mouse. Vis. Neurosci. *22*, 661–676.

Kadota, T., and Kadota, K. (1979). Filamentous contacts containing subjunctional dense lattice and tubular smooth endoplasmic reticulum in cat lateral geniculate nuclei. Brain Res. *177*, 49–59.

Kasthuri, N., Hayworth, K.J., Berger, D.R., Schalek, R.L., Conchello, J.A., Knowles-Barley, S., Lee, D., Vázquez-Reina, A., Kaynig, V., Jones, T.R., et al. (2015). Saturated Reconstruction of a Volume of Neocortex. Cell *162*, 648–661.

Krahe, T.E., El-Danaf, R.N., Dilger, E.K., Henderson, S.C., and Guido, W. (2011). Morphologically distinct classes of relay cells exhibit regional preferences in the dorsal lateral geniculate nucleus of the mouse. J. Neurosci. *31*, 17437–17448.

Lee, B.B., Virsu, V., and Creutzfeldt, O.D. (1983). Linear signal transmission from prepotentials to cells in the macaque lateral geniculate nucleus. Exp. Brain Res. *52*, 50–56.

Leventhal, A.G., Rodieck, R.W., and Dreher, B. (1981). Retinal ganglion cell classes in the Old World monkey: morphology and central projections. Science *213*, 1139–1142.

Lieberman, A.R. (1974). Comments on the fine structural organization of the dorsal lateral geniculate nucleus of the mouse. Anat. Embryol. (Berl). *145*, 261–267.

Ling, C., Hendrickson, M.L., and Kalil, R.E. (2012). Morphology, classification, and distribution of the projection neurons in the dorsal lateral geniculate nucleus of the rat. PLoS ONE *7*, e49161.

Marshel, J.H., Kaye, A.P., Nauhaus, I., and Callaway, E.M. (2012). Anterior-posterior direction opponency in the superficial mouse lateral geniculate nucleus. Neuron *76*, 713–720.

Martinez, L.M., Molano-Mazón, M., Wang, X., Sommer, F.T., and Hirsch, J.A. (2014). Statistical wiring of thalamic receptive fields optimizes spatial sampling of the retinal image. Neuron *81*, 943–956.

Mastronarde, D.N. (1992). Nonlagged relay cells and interneurons in the cat lateral geniculate nucleus: receptive-field properties and retinal inputs. Vis. Neurosci. *8*, 407–441.

Morgan, J.L., and Lichtman, J.W. (2013). Why not connectomics? Nat. Methods *10*, 494–500.

Ng, A., Jordan, M., and Weiss, Y. (2002). On spectral clustering: analysis and an algorithm. In Advances in Neural Information Processing Systems 14, T. Dietterich, S. Becker, and Z. Ghahramani, eds. (MIT Press), pp. 849–856.

Piscopo, D.M., El-Danaf, R.N., Huberman, A.D., and Niell, C.M. (2013). Diverse visual features encoded in mouse lateral geniculate nucleus. J. Neurosci. *33*, 4642–4656.

Poirazi, P., Brannon, T., and Mel, B.W. (2003). Pyramidal neuron as two-layer neural network. Neuron *37*, 989–999.

Rafols, J.A., and Valverde, F. (1973). The structure of the dorsal lateral geniculate nucleus in the mouse. A Golgi and electron microscopic study. J. Comp. Neurol. *150*, 303–332.

Sherman, S.M., and Spear, P.D. (1982). Organization of visual pathways in normal and visually deprived cats. Physiol. Rev. *62*, 738–855.

Spacek, J., and Lieberman, A.R. (1974). Ultrastructure and three-dimensional organization of synaptic glomeruli in rat somatosensory thalamus. J. Anat. *117*, 487–516.

Sretavan, D.W., Shatz, C.J., and Stryker, M.P. (1988). Modification of retinal ganglion cell axon morphology by prenatal infusion of tetrodotoxin. Nature *336*, 468–471.

Stanford, L.R., Friedlander, M.J., and Sherman, S.M. (1983). Morphological and physiological properties of geniculate W-cells of the cat: a comparison with X- and Y-cells. J. Neurophysiol. *50*, 582–608.

Sur, M., Esguerra, M., Garraghty, P.E., Kritzer, M.F., and Sherman, S.M. (1987). Morphology of physiologically identified retinogeniculate X- and Y-axons in the cat. J. Neurophysiol. *58*, 1–32.

Tapia, J.C., Wylie, J.D., Kasthuri, N., Hayworth, K.J., Schalek, R., Berger, D.R., Guatimosim, C., Seung, H.S., and Lichtman, J.W. (2012). Pervasive synaptic branch removal in the mammalian neuromuscular system at birth. Neuron *74*, 816–829.

Tavazoie, S.F., and Reid, R.C. (2000). Diverse receptive fields in the lateral geniculate nucleus during thalamocortical development. Nat. Neurosci. *3*, 608–616.

Usrey, W.M., Reppas, J.B., and Reid, R.C. (1999). Specificity and strength of retinogeniculate connections. J. Neurophysiol. *82*, 3527–3540.

Wilson, J.R., Friedlander, M.J., and Sherman, S.M. (1984). Fine structural morphology of identified X- and Y-cells in the cat's lateral geniculate nucleus. Proc. R. Soc. Lond. B Biol. Sci. *221*, 411–436.

Yeh, C.-I., Stoelzel, C.R., and Alonso, J.-M. (2003). Two different types of Y cells in the cat lateral geniculate nucleus. J. Neurophysiol. *90*, 1852–1864.

Zadeh, L.A. (1965). Fuzzy sets. Inf. Control *8*, 338–353.